

EM Pulse Scattering Front Echo Reduction for the Dielectric Elliptical Cylinder Located inside Dielectric Media

Emre İşcan* and Vasil Tabatadze

Informatics Institute of Istanbul Technical University, Istanbul, Turkey

ABSTRACT: This article presents a novel numerical approach to reduce scattering echoes in the front region of dielectric objects with the method of auxiliary sources. The method involves using a Gaussian radio pulse covering the 6–12 GHz frequency range. The approach involves optimizing the dimensions and dielectric permittivity of an elliptical cylinder in order to make it invisible, thus eliminating the need for metamaterial cloaking. The proposed approach has been validated by comparing the results of numerical experiments obtained during pulse echo observations with the FDTD and MoM numerical methods. The proposed method is a highly efficient and practical approach for scattering problems, such as scattering echo reduction, offering comparable results to FDTD and MoM methods with significantly reduced computational requirements.

1. INTRODUCTION

In recent years, notable progress has been made in the advancement of radar-based detection and EM cloaking technologies across various media, including inside ground, water, and other specialized medias. These efforts aim to enhance stealth capabilities, reduce detection risks, and improve the overall effectiveness of military, security, and civilian applications. Due to these factors, scientists have directed their endeavors towards investigating solutions in this particular domain. Many research studies have been conducted aiming to minimize detection risks and enhance invisibility capabilities, focusing on reducing radar cross-section [1] and discovering cloaking methods [2]. The study [3] presents a gradient-based optimization method using Maxwell's equations for reducing radar cross section through shape and material modifications. The study in [4] employs the 2-D ADE-FDTD method to analyze bistatic radar cross section of a plasma-coated airfoil. It shows that the optimizing plasma frequency and collision frequency can improve backscattering invisibility and reduce RCS at certain angles for bending airfoils. In paper [5] the straight-forward radar cross section suppression structure is proposed, utilizing only a dielectric superstrate with varying loadings to achieve wideband backscattering reduction. In paper [6], a technique is introduced for reducing the radar cross section of rod-like targets over a wide bandwidth. The method involves using multistep cylindrical structures with different radius to create a phase reversal that cancels backscattering. The study in [7] discusses recent developments in artificially structured metamaterials, focusing on a non-magnetic cylindrical cloak designed to operate at optical frequencies. The research [8] presents analytical models for mantle cloaking of electrically large objects, using the two-sided surface impedance method to analyze a cloak composed of a dielectric cylinder with an in-

ner PEC surface and an outer surface coated with metasurfaces, aiming to achieve scattering reduction. The study [9] explores metasurface that is polarization-insensitive and has angular stability, designed to achieve radar cross-section reduction over a range from 7 to 12 GHz.

These mentioned studies generally involve providing invisibility in all directions through the different types of coating materials and this make it complex to make object invisible in wide frequency range. Researchers often neglect geometric optimization and primarily concentrating on cloaking metallic objects. In the literature review, no study has been encountered on the topic of invisibility achieved through the optimization of dielectric object parameters inside the ground or any other layered medium with the purpose of reducing the echo in the front region. What distinguishes our current work from other studies is the specific idea of optimizing the dimensions and dielectric properties to minimize the reflection in the front region when an object is located in a hostile environment, as example landmine inside the ground. This is especially significant because a majority of modern landmines are constructed using dielectric materials. In that sense our study is unique. We focus on the scattering echo reduction in the front area because the echo in the back area, even it is big, is directed backward and can be absorbed by the ground below object. So, it will not reach the sensor located above ground.

Continuing from the previous studies [10, 11], this study introduces a novel Gaussian radio pulse echo observation method based on the method of auxiliary sources (MAS) aimed at mitigating scattering front echoes caused by dielectric objects within the broadband frequency range of 6–12 GHz. The method involves a unique approach of optimizing the ellipse's dimensions and dielectric permittivity to reduce front echo, which eliminates the necessity for metamaterial cloaking.

This technique exhibits remarkable efficiency over a wide frequency spectrum, providing invisibility at different incident

* Corresponding authors: Emre İşcan (emre.iscan@itu.edu.tr).

angles as well. This study can be useful for engineers for designing undetectable dielectric landmines.

2. THE PROBLEM FORMULATION

2.1. Analysis of the Problem from a Time Domain Approach

The content of this section presents the mathematical formulation for reducing the scattering echoes from the dielectric objects located inside the ground or other environments in the front region. The Gaussian radio pulse used as the incident field is specified in formula (1):

$$E^{inc}(\rho, t = jT) = \sum_{i=-\infty}^{\infty} \frac{e^{-\alpha^2(\frac{t}{c} + iT)^2}}{\sqrt{\rho}} \cos(\omega_{\max}(iT))\delta[i - j], \quad j = -\infty \text{ to } \infty \quad (1)$$

In the formula $\rho = \sqrt{(x - x_{inc})^2 + (y - y_{inc})^2}$ calculates the distance between an observation point (x, y) and a source location (x_{inc}, y_{inc}) in a two-dimensional space. δ is the Kronecker's delta function. The electric field polarization is along the z direction.

In formula (1), specific symbols are utilized to represent different parameters. The speed of light is denoted as c , the period as T , and the parameter α^2 controls the pulse's time width. Its unit is sec^{-2} . Once the Fourier coefficient of the incident wave has been obtained, the direct problem is tackled for each frequency separately. Later, the solution for the scattered field is multiplied by the Fourier coefficients of the incident wave. The behavior of the field in the time domain can be determined by combining the resulting values across all frequencies. There are total of two scatterers, consisting of a ground plane and an elliptical object inside the ground. Considering that the scatterers are dielectrics, the boundary conditions of the electric and magnetic fields are satisfied on both scatterers surfaces for each different frequency. The detailed information about obtaining the distribution of scattered fields at each frequency is given under the next subsection.

2.2. Solution of the Direct Problem Using the MAS

The stated problem is addressed using the method of auxiliary sources. This particular method has the benefit of effectively handling the singularity problems that could emerge when the observation and source points coincide within the integral derived from the boundary conditions [15]. The geometry of the problem includes the contours \vec{r}_p and \vec{r}_e , which represent the physical interfaces of ground plane and elliptical object inside the ground, respectively, as shown in Figure 1. The solid lines represent the physical contours. The round dotted lines are used to illustrate the auxiliary contours. Medium I corresponds to a free space, medium II represents the dielectric media, and medium III stands for the area inside of the elliptic object. To address the direct problem, we introduce the auxiliary sources. Their coordinates are denoted by the \vec{r}_{p_in} , \vec{r}_{p_out} , \vec{r}_{e_in} , \vec{r}_{e_out} . The auxiliary sources located on the contour \vec{r}_{p_in} are responsible for generating the field in medium I, while the auxiliary sources on the contour \vec{r}_{p_out} and \vec{r}_{e_in} create the field in

medium II. Finally, the auxiliary sources located on the contour \vec{r}_{e_out} are responsible for generating the field in medium III.

The incident source location $\vec{r}_{inc} = (x_{inc}, y_{inc}) = (d_{inc} \cdot \sin(\theta), d_{inc} \cdot \cos(\theta))$.

TABLE 1. Parameters and their corresponding values.

Parameter	Value	Parameter	Value
ε_g	2	\mathbf{d}_{p_out}	0.01 m
ε_e	4	d_{p_in}	0.01 m
d	0.1 m	d_{e_out}	$\min(R_1 R_2) * 0.3 \text{ m}$
N_e	100	d_{e_in}	$\min(R_1 R_2) * 0.3 \text{ m}$
N_p	200	d_{inc}	1.7 m

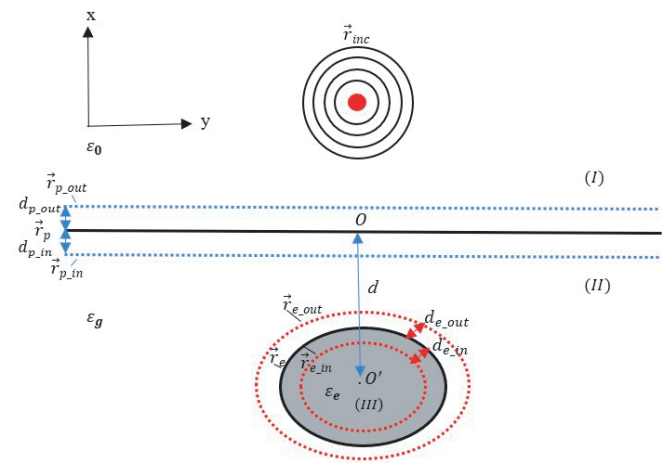


FIGURE 1. The geometry of the problem.

N_e stands for the number of discretization points used to model the cylinder. N_p stands for the number of discretization points used to model the plane. d represents the distance between the origin of frame reference O and the center of elliptical cylinder O' . R_1 and R_2 are the semi axes of the ellipse. Size of the plane is taken 1 m. Considering the area of field calculation and the size of the elliptical object this size is big enough. The location of the incident source is: $\vec{r}_{inc} = (1.7 \cdot \cos(\theta), 1.7 \cdot \sin(\theta))(\text{m})$. $\theta = \frac{\pi}{2}, \frac{\pi}{3}, \frac{\pi}{4}, \frac{\pi}{6}$. The parameters d and ε_g given in the table are unchanged throughout the study.

Medium I defined by ε_0 relative permittivity is vacuum. Medium II is indicated by a relative permittivity denoted by ε_g . Also, the dielectric material has a relative permittivity represented by ε_e . Outer auxiliary surface sources are used to describe the field inside the object, while inner auxiliary surface sources are employed to characterize the field outside the object. The expression for the scattered electric field in the media I is given by formula (2):

$$E_{p_in}(\vec{r}) = \sum_{n=1}^{N_p} X_n^{p_in} H_0^{(1)}(k_o |\vec{r} - \vec{r}_{p_in}|) \quad (2)$$

In this context, we have $H_0^{(1)}$ representing the Hankel functions of the 1st kind and 0th order. The X_n^{p-in} corresponds to the unknown complex amplitudes of the auxiliary sources, which are positioned on the inner auxiliary contour. Also, k_0 denotes the wave number of the vacuum. In the media II electric field is described by the outer auxiliary sources of the plane and by the inner auxiliary sources of the elliptical object. The electric field represented by the outer sources of the plane is given by the formula (3):

$$E_{p_out}(\vec{r}) = \sum_{n=1}^{N_p} X_n^{p-out} H_0^{(1)}(k_g |\vec{r} - \vec{r}_{p-out}|) \quad (3)$$

X_n^{p-out} represents the unknown complex coefficients of the auxiliary sources that are distributed across the outer auxiliary contour of the plane. k_g represents the wave number of the media II. The electric field represented by the inner auxiliary sources of the elliptical object is given in formula (4).

X_n^{e-in} corresponds to the unknown complex amplitudes of the auxiliary sources, which are positioned on the inner auxiliary contour of the ellipse.

$$E_{e_in}(\vec{r}) = \sum_{n=1}^{N_e} X_n^{e-in} H_0^{(1)}(k_e |\vec{r} - \vec{r}_{e-in}|) \quad (4)$$

The formula for the electric field inside the elliptical object is given by (5):

$$E_{e_out}(\vec{r}) = \sum_{n=1}^{N_e} X_n^{e-out} H_0^{(1)}(k_e |\vec{r} - \vec{r}_{e-out}|) \quad (5)$$

X_n^{e-out} describes the unknown complex coefficients of the auxiliary sources that are distributed across the outer auxiliary contour of the ellipse. Meanwhile, k_e represents the wave number inside the ellipse.

The incident field is defined in the medium I and is expressed as:

$$E_{inc}(\vec{r}) = H_0^{(1)}(k_0 |\vec{r} - \vec{r}_{inc}|) \quad (6)$$

The method used to express the magnetic field components inside and outside the scatterer is analogical. Using Maxwell's Eq. (7), we can derive the expression for the magnetic field.

$$\text{rot} \vec{E} = -i\omega\mu \vec{H} \quad (7)$$

Here, the symbol ω is used to denote the angular frequency, while μ is employed to represent the permeability. Moreover, the term rot pertains to the curl operator. In order to determine the unknown complex amplitudes in the field expressions, it is necessary to apply the boundary conditions as follows (8)–(11):

$$\begin{aligned} & E_{p_in}(\vec{r}_p(i)) + E_{inc}(\vec{r}_p(i)) \\ &= E_{p_out}(\vec{r}_p(i)) + E_{e_in}(\vec{r}_p(i)) \end{aligned} \quad (8)$$

$$E_{p_out}(\vec{r}_e(j)) + E_{e_in}(\vec{r}_e(j)) = E_{e_out}(\vec{r}_e(j)) \quad (9)$$

$$\begin{aligned} & H_{p_in}(\vec{r}_p(i)) \tau_P(i) + H_{inc}(\vec{r}_p(i)) \tau_P(i) \\ &= H_{p_out}(\vec{r}_p(i)) \tau_P(i) + H_{e_in}(\vec{r}_p(i)) \tau_P(i) \end{aligned} \quad (10)$$

$$\begin{aligned} & H_{p_out}(\vec{r}_e(j)) \tau_e(j) + H_{e_in}(\vec{r}_e(j)) \tau_e(j) \\ &= H_{e_out}(\vec{r}_e(j)) \tau_e(j) \end{aligned} \quad (11)$$

The variable i ranges from 1 to N_p , and the variable j ranges from 1 to N_e . From the formulations given above (8)–(9) define the electric field boundary condition in the plane and the

elliptical object, respectively. Formulations (10)–(11) define the magnetic field boundary condition on the plane and the elliptical object, respectively. Here, $\tau_P(i)$ represents the tangential component of the plane, and $\tau_e(j)$ stands for the tangential component of the elliptical object. Therefore, the continuity of the tangential components of the total electric and magnetic fields must be ensured at each contour. Once the electric and magnetic fields' boundary conditions are satisfied, the system of formulations (8)–(11) gives rise to a set of linear algebraic equations. By performing inversion procedure on these equations, the amplitudes of the unknowns can be determined. The direct problem is solved for each frequency component of the incident pulse, allowing us to determine the field values inside and outside of the object. Afterwards, these calculated values are multiplied by the complex amplitudes of the spectrum and the exponential term $e^{-i\omega t}$, and then summed up. As a result, the total field in the time domain is determined for a particular point in space and time. This approach allows for the calculation of the pulse echo at a specific point.

3. NUMERICAL RESULTS

The analysis of the numerical experiments and their corresponding results centers on the evaluation of the echo distributions of the scattered electric field for both dielectric media and the elliptical object inside this media under various scenarios. Subsequently, specific values of the total field are given for a particular observation point in time. As we mentioned above the incident wave has the form of a Gaussian radio pulse. The period of the pulse T for the numerical experiments is set as 9 nanoseconds. In formula (1), the value of $\alpha^2 = (\frac{1}{64}) \times 10^{21} \text{ sec}^{-2}$.

Scattering echoes in the front area can be reduced by optimizing various parameters, such as adjusting the dimensions and dielectric permittivity of an elliptic dielectric object. Dielectric objects tend to produce more echoes at their resonant frequency range. To address this, a Gaussian radio pulse is used, covering a wide frequency range from 6 to 12 GHz, occupying multiple resonances. Figure 2(a), shows the total radar cross-section of the elliptical cylinder measured in meters. As we see the cylinder has many resonances throughout given frequency range.

Consequently, by deliberately choosing frequencies within this specific interval for the incident pulse spectrum, one can ensure a notable amplification of echo signals enhancing the efficiency of signal detection and analysis.

ω_{\max} has been chosen as 9 GHz. Figure 2(b) provides the near field distribution at the resonance value $f = 8.6689$ GHz. We can see the high field values on the contour of the cylinder. In this scenario the object is located in the infinite dielectric media. $\vec{r}_{inc} = (-1000, 0)$ (m).

The program package developed in MATLAB has been utilized to solve the diffraction problem based on the above-described algorithm. This program package generates an animation [12] that visualizes the evolution of the electromagnetic field on a 2D plane as a Gaussian radio pulse signal interacts with an elliptical scattering object. The animation shows how the field changes over time due to the scattering process. We optimize the incident field parameters and carefully adjust the

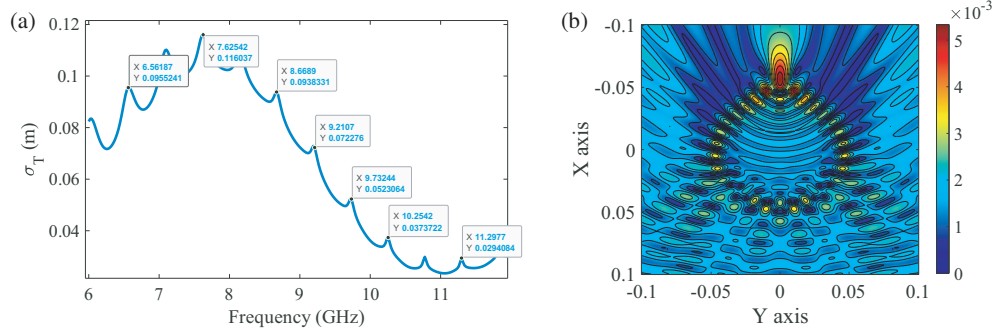


FIGURE 2. Total radar cross section inside ground (a) $R_1 = 0.05$ m, $R_2 = 0.05$ m, $\epsilon_g = 2$, $\epsilon_e = 4$, (b) Resonance field distribution at the frequency $f = 8.6689$ GHz.

source location and object parameters to achieve the front echo minimization.

During the pulse echo observations, for an effective reduction of scattering front echoes, critical parameters such as the dimensions and dielectric permittivity of an elliptical cylinder need to undergo a precise optimization process.

As an example, for the not optimized parameters, the front echo distributions are shown in Figure 3. In Figure 3(a), a significant maximum front echo formation is observed at the center. In Figure 3(b), there are a total of 3 front echoes, one at the center and the other two shifted to the sides. Subsequently, as seen in Figure 3(c), the existing front echo is minimized at the center and predominantly reflects towards the right and left sides. This approach demonstrates that larger maximum front echoes can be effectively controlled and reduced in pulse echo by changing the dielectric parameters. After pulse echo analyses, a series of optimization processes were conducted to reduce the detected front echoes by optimizing parameters such as the dimensions and dielectric permittivity of the elliptical cylinder.

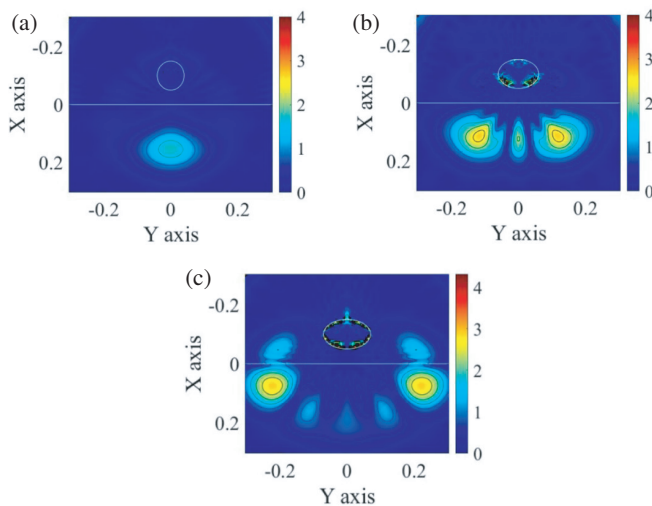


FIGURE 3. Echo field distributions ($\epsilon_e = 6$, $\theta = \frac{\pi}{2}$) for (a) $R_1 = 0.03$ m, $R_2 = 0.02$ m, (b) $R_1 = 0.03$ m, $R_2 = 0.04$ m, (c) $R_1 = 0.03$ m, $R_2 = 0.05$ m.

The generated animations [12] provided insights into the scattering process due to the interaction between an elliptical

object inside the ground and a Gaussian radio pulse, and it demonstrated how the echo behaves for 180 different scenarios evolved over time. For obtaining these 180 videos we changed permittivity in the range 1 to 5 with the step 1. We changed semi axes values between 0.01 and 0.06 with the step 0.01. From these 180 videos we chose the best ones: $\epsilon_e = 5$, $R_1 = 0.02$ m, $R_2 = 0.05$ m and $\epsilon_e = 6$, $R_1 = 0.02$ m, $R_2 = 0.05$ m. For all these 180 cases $\theta = \frac{\pi}{2}$. After that for these optimized values of parameters we calculated results for different incidence angles such as $\theta = \frac{\pi}{2}, \frac{\pi}{3}, \frac{\pi}{4}, \frac{\pi}{6}$, it can be observed from the snapshots obtained from animations that Gaussian radio pulses create comparatively small echo in the front region, as shown in Figure 4.

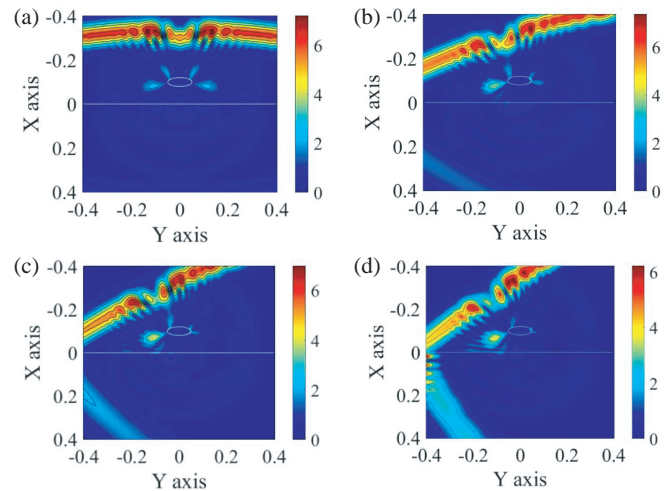


FIGURE 4. Optimized echo field distributions ($\epsilon_e = 5$, $R_1 = 0.02$ m, $R_2 = 0.05$ m) for (a) $\theta = \frac{\pi}{2}$, (b) $\theta = \frac{\pi}{3}$, (c) $\theta = \frac{\pi}{4}$, (d) $\theta = \frac{\pi}{6}$.

Findings obtained from different perspectives demonstrate that every situation creates a unique and non-replicable echo of its own. The results of another research study conducted for various incidence angles and optimized elliptical cylinder parameters are presented in Figure 5. In Figure 5, it can be seen that the reduction of the echo amplitudes takes place specifically in the front region as a result of the parameters' optimization.

By optimizing the object's parameters, the echo of the gaussian radio pulse in the frontal region of the scatterers is signifi-

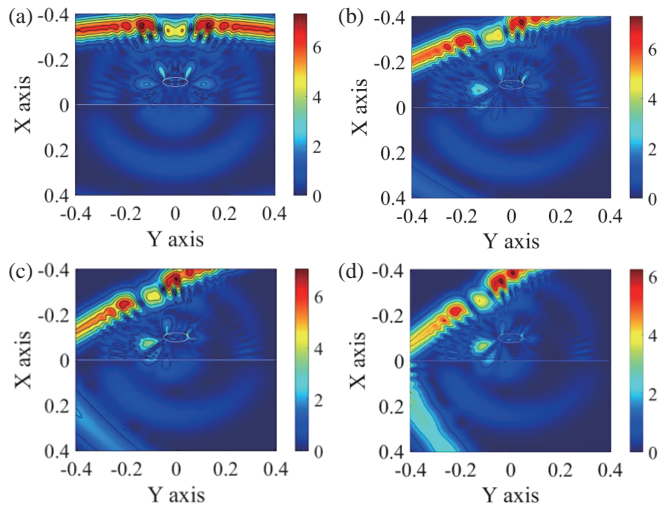


FIGURE 5. Optimized echo field distributions ($\epsilon_e = 6$, $R_1 = 0.02$ m, $R_2 = 0.05$ m) for (a) $\theta = \frac{\pi}{2}$, (b) $\theta = \frac{\pi}{3}$, (c) $\theta = \frac{\pi}{4}$, (d) $\theta = \frac{\pi}{6}$.

cantly reduced as seen in comparison of the Figure 3 with Figures 4–5. This achievement holds considerable significance for practical applications, where placing sensors behind the object for measurements is not feasible. This method exhibits exceptional efficiency over a wide frequency range and ensures invisibility at different incidence angles as well. As a result, the proposed approach presents a practical numerical method with versatile applications in military and industrial settings. It can be utilized for stealth and invisibility technology, missile guidance, and more, effectively reducing echoes in the front region of the object.

4. COMPARISON WITH OTHER METHODS

The obtained results with MAS have been compared with the finite difference time domain (FDTD) and method of moments (MoM) numerical methods, and the accuracy of the proposed method has been demonstrated. The method comparison has been conducted at 2 GHz. We chose this specific frequency because in FDTD code we solve 3D problem with actual 3D cylinder which for higher frequencies required too much computational time.

Figure 6 demonstrates a comparison of the magnitudes of electric field distributions between the suggested approach (a) and the FDTD method (b).

While calculating with FDTD we put the media II with finite length which causes some back reflections and as a result it gives some deviation from the MAS results. But still, we see very good match in the field features. It is important to highlight that the suggested approach requires less than 1 minute to yield the result, whereas the FDTD method, while achieving comparable accuracy, takes approximately 10 minutes to compute the same outcome.

We assume that if at one frequency we have a good match we will get good match for gaussian pulse also because the pulse is the combination of multiple frequencies.

Figure 7 illustrates a comparative analysis of the electric field distributions between the MAS (a) and the Method of Moments

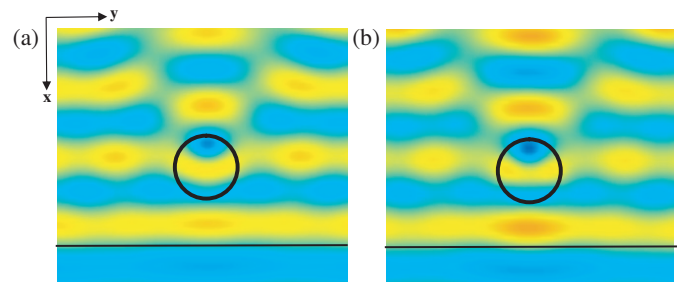


FIGURE 6. Comparison of MAS and FDTD field distributions (a) MAS circle in the ground ($R = 0.05$ m, $\epsilon_{gr} = 4$, $\epsilon_{cir} = 2$, $f = 2$ GHz), (b) FDTD circle in the ground ($R = 0.05$ m, $\epsilon_{gr} = 2$, $\epsilon_{cir} = 4$, $f = 2$ GHz).

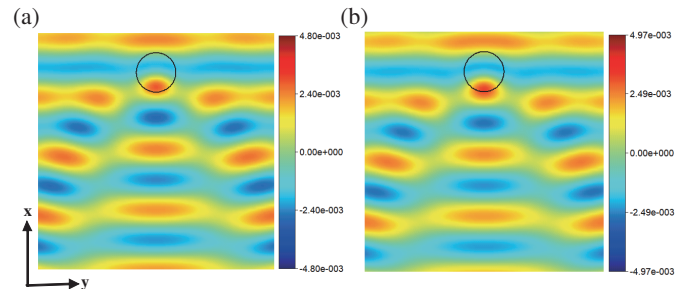


FIGURE 7. Comparison of MAS and MoM field distributions (a) MAS circle in free space ($R = 0.05$ m, $\epsilon = 2$, $f = 2$ GHz), (b) MoM circle in free space ($R = 0.05$ m, $\epsilon = 2$, $f = 2$ GHz).

(MoM) (b). The suggested approach has been found to calculate results faster than the MoM method while achieving comparable accuracy in obtaining the same result.

These results have demonstrated that the proposed approach is efficient in terms of computation, especially for scattering problems where FDTD and MoM require more computational resources and longer time to achieve comparable results.

5. CONCLUSION

This article proposes a novel numerical strategy aimed at reducing scattering front echo around dielectric objects located in the ground or other media. The approach involves utilizing a Gaussian radio pulse with a frequency range of 6–12 GHz and optimizing an ellipse’s dimensions and dielectric permittivity. By doing so, the need for metamaterial cloaking is eliminated. This method demonstrates impressive effectiveness across a broad range of frequencies, enabling invisibility from various incidence angles as well. This is the first study presented in terms of optimization to reduce scattering echoes around dielectric elliptical cylinder in the dielectric media in order to make dielectric objects invisible. The animations [12] obtained with the developed code showcase the remarkable capabilities of the program in visualizing the field distribution with reduced front echoes and improved invisibility. The effectiveness of the suggested method has been confirmed through a comparison of results from numerical experiments conducted at specific frequency using both FDTD and MoM numerical methods. Unlike FDTD and MoM methods, this novel approach achieves comparable results with significantly reduced computational requirements.

The implications of this advancement are substantial, as it holds great promise for invisibility and stealth technologies by reducing the scattering front echo for practical applications.

REFERENCES

- [1] Murugesan, A., K. T. Selvan, A. K. Iyer, K. V. Srivatsav, and A. Alphones, "A review of metasurface-assisted RCS reduction techniques," *Progress In Electromagnetics Research B*, Vol. 94, 75–103, 2021.
- [2] Alitalo, P. and S. Tretyakov, "Electromagnetic cloaking with metamaterials," *Materials Today*, Vol. 12, No. 3, 22–29, 2009.
- [3] Bondeson, A., Y. Yang, and P. Weinerfelt, "Optimization of radar cross section by a gradient method," *IEEE Transactions on Magnetics*, Vol. 40, No. 2, 1260–1263, March 2004, doi: 10.1109/TMAG.2004.824730.
- [4] Du, F., P. Huang, and J. Ji, "Study and optimization on the scattering characteristic of two-dimensional metal airfoil covered with plasma using ADE-FDTD," *Optik*, Vol. 147, 224–231, 2017.
- [5] Liao, W. J., Y. C. Hou, and S. T. Chen, "Dielectric-loaded ultrawideband RCS reduction structures," *IEEE Transactions on Antennas and Propagation*, Vol. 68, No. 3, 2277–2289, March 2020, doi: 10.1109/TAP.2019.2948703.
- [6] Chen, S. H., Y. C. Hou, and W. J. Liao, "Multistep cylindrical structure design for wideband radar cross section reduction at normal incidence," *IEEE Transactions on Antennas and Propagation*, Vol. 63, No. 4, 1849–1853, April 2015, doi: 10.1109/TAP.2015.2394804.
- [7] Cai, W., U. Chettiar, A. Kildishev, and V. Shalaev, "Optical cloaking with metamaterials," *Nat Photonics*, Vol. 1, 224–227, Birck and NCN Publications, 2007.
- [8] Younesiraad, H., M. Bemani, and S. Nikmehr, "Scattering suppression and cloak for electrically large objects using cylindrical metasurface based on monolayer and multilayer mantle cloak approach," *IET Microwaves, Antennas & Propagation*, Vol. 13, No. 3, 278–285, 2019.
- [9] Song, Y. C., J. Ding, C. J. Guo, Y. H. Ren, and J. K. Zhang, "Ultra-broadband backscatter radar cross section reduction based on polarization-insensitive metasurface," *IEEE Antennas and Wireless Propagation Letters*, Vol. 15, 329–331, 2016, doi: 10.1109/LAWP.2015.2443853.
- [10] Tabatadze, V., K. Karaçuha, and R. Zaridze, "Electromagnetic diffraction by a pulse from 2-D dielectric objects," *2022 IEEE 2nd Ukrainian Microwave Week (UkrMW)*, 559–562, Ukraine, 2022, doi: 10.1109/UkrMW58013.2022.10037102.
- [11] Tabatadze, V., O. Drobakhin, and K. Karaçuha, "Pulse diffraction by a circular dielectric cylinder," *Journal of Electrical Engineering*, Vol. 74, No. 3, 188–196, 2023, <https://doi.org/10.2478/jee-2023-0025/>.
- [12] <https://www.youtube.com/channel/UCc-HE2OgIpftQP096haA6Hw>.